Hidden star formation in the early Universe

Leeuwen, I. F. van

1 Introduction

1.1 A brief history of the Universe

Today, the most widely accepted description of the Universe is provided by the dark energy and cold dark matter (ΛCDM) model. In this framework, the Universe began with a hot Big Bang, when the Universe was extremely dense and nearly homogeneous. The deviations from this homogeneity were small quantum fluctuations, which initiated structure formation through the density perturbations they introduced. These density perturbations grew significantly in size during inflation, a period of exponential expansion lasting only a fraction of second.

After inflation, the Universe kept expanding, albeit at a slower rate, and the hot plasma of particles arising from the Big Bang gradually cooled. At this stage the Universe was still opaque, as light and matter were tightly coupled due to the scattering of photons by electrons. About 380,000 years after the Big Bang the plasma cooled enough for protons and electrons to combine into neutral atoms. Subsequently, photons were able to travel freely through the Universe. The decoupling of light and matter produced the last scattering surface, the cosmic microwave background (CMB).

Meanwhile, density perturbations continued to grow under the influence of gravity from dark matter. As the Universe expanded, the density of perturbations became much higher than the average density. These critically dense peaks collapsed and formed gravitationally bound dark matter halos. The process of structure formation is hierarchical: small halos form first and grow into larger dark matter halos through the accretion of matter and mergers (White & Rees 1978).

Within these dark matter halos, gas accumulated and cooled radiatively. Once the gas had a sufficiently low temperature, it gathered at the center of the halo's potential well. When the gas's self-gravity overcame the gravity from the dark matter, it collapsed to form the first stars. The formation of the first stars commenced a few hundred million years after the Big Bang, consequently giving rise to the formation of the first galaxies.

The ionizing radiation of stars, galaxies, and active galactic nuclei (AGNs) gradually lead to the Universe's most recent major phase transition: the Epoch of Reionization (EoR). The EoR ended when the Universe was fully ionized, at a redshift (z) of around 6 (Wise 2019), while galaxies continued to form and evolve to the present day. The evolution of the Universe is illustrated in Figure 1.1, from the Big Bang to the present day.

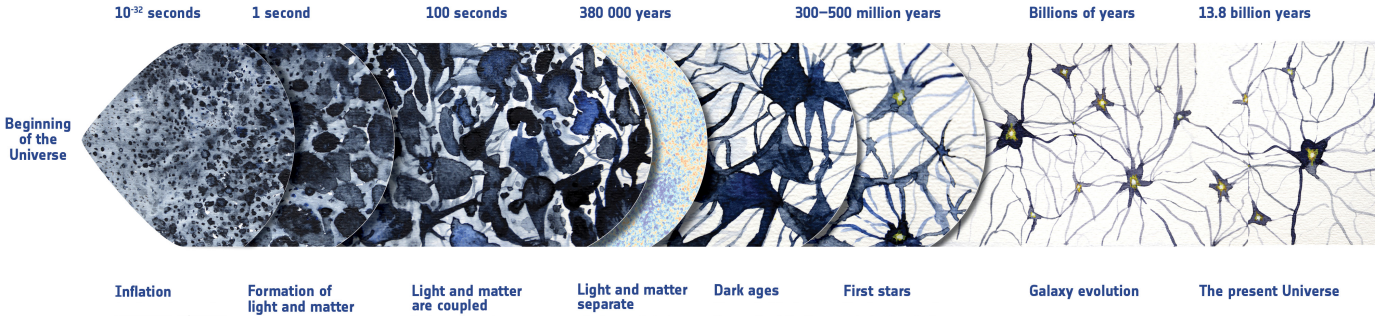

Figure 1.1: A schematic overview of the history of the Universe from the Big Bang to the present day. The Universe expanded exponentially during inflation and afterwards continued expanding at a slower rate. About 380,000 years after the Big Bang, light and matter decoupled and photons traveled freely generating the cosmic microwave background. Subsequently, the Universe was in the Dark ages, until the formation of the first stars and galaxies. Figure is adapted from ESA (`https://sci.esa.int/s/WXJdq1A`).

1.2 Galaxy evolution: star formation through cosmic time

At the present day, we observe a diverse population of galaxies. In the local Universe, galaxies exhibit a tight correlation between stellar mass and star formation, known as the star-forming main sequence, also persistent at high redshift (e.g. Speagle et al. 2014; Schreiber et al. 2015). Galaxies that deviate from this relation are either rapidly forming stars (starburst galaxies) or experience a decline in star formation activity (quiescent galaxies).

Comprehending the evolution of the galaxy population as a whole, especially regarding the galaxies in the first billion years of the Universe, is fundamental to our understanding of the Universe (Madau & Dickinson 2014). Galaxies are the primary objects in which star formation in the Universe takes place. Therefore, to study galaxy evolution, examining star formation across cosmic time is essential. However, estimating the star formation rate (SFR) of a galaxy from the observed light is not straightforward, especially at high redshift.

1.2.1 Spectral energy distribution

A galaxy hosts a variety of stellar populations, composed of stars with different masses, ages and metallicities. In nearby galaxies, it is possible to resolve individual stars and directly infer the stellar populations responsible for the observed light. At high redshift, however, it is impossible to observe the actual distribution of stars. Instead, the integrated light of many stellar populations is observed, making it essential to grasp how each of them contribute to a galaxy spectrum.

For this purpose, stellar evolution models are developed for stars of a given initial mass and composition, which is the first component needed to construct models of the spectral energy distribution (SED) of a galaxy. The initial mass function (IMF), which describes the distribution of stellar masses within a stellar population, is the second key ingredient needed for the modeling of integrated light of a galaxy. Commonly adopted IMFs (e.g. Salpeter 1955; Kroupa 2001; Chabrier 2003) predict that low-mass stars are far more abundant than massive stars. The third and final component required is the star formation history (SFH), which describes the star formation rate as a function of time. SFHs are often parametrized, for example as a star formation rate that declines exponentially with cosmic time. By combining stellar evolution models, an assumed IMF and a SFH, the integrated light of a galaxy is modeled. This modeling of the SED also provides a means to infer the stellar mass by constraining the mass-to-light ratio.

In Figure 1.2 we present the SED of a dusty mock galaxy ($A_V = 2$,

i.e. an extinction of two magnitudes in the V band). A distinct feature in galaxy spectra is the Lyman-alpha transition at < 1216 Å, produced by the absorption of short wavelength photons by neutral hydrogen. Redward of this is the rest-frame ultraviolet (rest-UV) emission, dominated by massive, short lived stars ($\lesssim 100$ Myr; Kennicutt 1998). At longer wavelengths, in the optical and near-infrared, the light is dominated by low-mass stars which comprise the bulk of the stellar mass. Moving into the far-infrared regime of the spectra the emission from dust becomes prominent, often referred to as the dust SED.

Dust is a fundamental component of galaxies: it is a byproduct of star formation and crucial for the thermodynamics and chemistry of the interstellar medium (ISM) (Draine 2003). It is thought that dust is mostly composed of small silicates and carbonaceous particles. In the early Universe, it is believed that dust is mainly produced by core collapse supernovae and asymptotic giant branch (AGB) stars. Because dust grains are most efficient at absorbing light with short wavelengths, rest-UV emission is attenuated in the presence of dust. Rest-UV observations alone can therefore be insufficient probes of star formation, as dust may hide a significant fraction of star formation. However, dust is heated by the absorption of the photons and then reradiates the energy in the infrared, providing a way to observe obscured star formation.

1.2.2 Star formation rate tracers

The star formation rate describes how rapidly a galaxy forms stars, typically estimated in solar masses per year. Rather than measuring an instantaneous rate, SFRs are often averaged out over longer timescales (e.g. ~ 100 Myr). The star formation rate of a galaxy provides insight into its ISM conditions and potential evolutionary path. Several observational tracers can be utilized to estimate the SFR. In this thesis we will focus on several different probes which we introduce in the subsections to follow.

1.2.2.1 Rest-ultraviolet emission

One of the most widely used tracers of star formation is rest-ultraviolet emission. Rest-UV light is dominated by massive stars with lifetimes of less than 100 Myr and therefore efficiently traces recent star formation. In fact, the rest-UV luminosity is found to scale linearly with the SFR (Kennicutt 1998). The rest-UV continuum emission is typically measured at 1500 Å, such that absorption features in the Lyman forest at shorter wavelengths and contamination from older stellar populations at longer wavelengths are avoided (Kennicutt 1998). To convert the observed rest-UV luminosity into a SFR requires an assumption on the IMF, to account for the full distribution of stars, including low-mass stars. Rest-UV light, however, may suffer

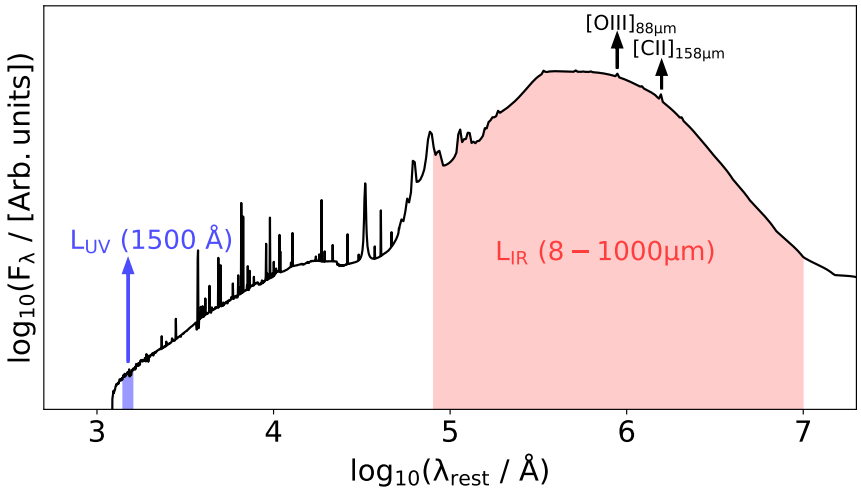

Figure 1.2: The spectral energy distribution of a dusty mock galaxy ($A_V = 2$ mag) generated with the SED modeling code BAGPIPES (Carnall et al. 2018). Two wavelength ranges are of particular importance to this thesis: the rest-ultraviolet (rest-UV) emission at ~ 1500 Å and the infrared (IR) emission at $8 - 1000$ μm. The rest-UV and IR luminosities are used to trace the unobscured and obscured star formation rates, respectively. Additionally, bright far-IR emission lines such as $[\mathrm{OIII}]_{88\mu\mathrm{m}}$ and $[\mathrm{CII}]_{158\mu\mathrm{m}}$ can be utilized to trace the total star formation rate, as they are unaffected by dust attenuation.

significant attenuation in the presence of dust, leading to an underestimate of the total SFR. For this reason, the SFR as traced by rest-UV emission is referred to as the **unobscured SFR**.

1.2.2.2 Infrared emission

The absorbed rest-UV photons heat the dust in galaxies, which subsequently re-emits this energy in the infrared (IR). Since the rest-UV emission traces recent star formation and IR emission probes the reprocessed emission, the IR luminosity traces the **dust-obscured star formation rate**.

The total IR luminosity is defined as the integral of the SED between 8 μm to 1000 μm. Ideally, to robustly sample the shape of the dust SED multiple IR continuum observations are used. However, at high redshift often continuum measurements in only one frequency band are available. Consequently, assumptions need to be made on the shape of the dust SED, which is typically modeled as a modified blackbody. This blackbody is parametrized by the dust emissivity index ($\beta_{\rm em}$, that mainly controls the slope of the Rayleigh-Jeans tail) and dust temperature ($T_{\rm dust}$, which moves the peak of the dust SED to shorter wavelengths for higher temperatures). The observed continuum flux at a specific wavelength is then used to rescale the dust SED, which is integrated to obtain the IR luminosity.

To convert the IR luminosity to an obscured star formation rate the assumption is made that the IR emission is the result of recent star formation, without a contribution from an AGN or older stellar population (De Looze et al. 2014). The infrared excess ($\mathrm{IRX} = \frac{L_{\rm IR}}{L_{\rm UV}}$) as a function of the UV continuum slope (e.g. Meurer et al. 1999) is an empirical relation widely used to correct rest-UV luminosities for dust attenuation. Such relations are much more uncertain at high redshift, in part due to the complex distributions of stars and dust, which are not always co-spatial. Rather than relying on such relations, the total SFR can be estimated by combining the contributions from unobscured (rest-UV) and obscured (IR) star formation.

1.2.2.3 Far-IR fine structure lines

An alternative measurement of the star formation rate can be provided by emission lines. While continuum measurements often require deep integrations, emission lines are sometimes more readily detected and have therefore attracted interest as a tracer of star formation. In particular, far-infrared emission lines are well suited for this purpose, as they are expected to be unaffected by dust attenuation, therefore showing potential as a tracer for the **total star formation rate**. Two of the brightest far-IR emission lines at high redshift are the fine structure lines $[\mathrm{CII}]_{158\mu\mathrm{m}}$ and $[\mathrm{OIII}]_{88\mu\mathrm{m}}$[1], routinely used to spectroscopically confirm redshifts.

[1]For simplicity we refer to $[\mathrm{CII}]_{158\mu\mathrm{m}}$ and $[\mathrm{OIII}]_{88\mu\mathrm{m}}$ as [CII] and [OIII], respectively.

With roughly 700 [CII] observations of $z \gtrsim 4$ sources, it is the most commonly used emission line for the identification and characterization of galaxies in the early Universe (Decarli & Díaz-Santos 2025). Neutral carbon ([CI]) has a low ionization potential of 11.3 eV and is therefore relatively easy to excite. Neutral hydrogen has an ionization potential of 13.6 eV, thus singly ionized carbon ([CII]) can trace both the neutral and ionized gas of a galaxy. The majority of [CII] emission in star-forming galaxies is found to originate from the neutral gas in photodissociation regions (PDRs) (Stacey et al. 2010; Wolfire et al. 2022). [CII] is the main coolant of neutral gas, which is heated by recent star formation. It is therefore expected to trace the SFR and to be especially bright in star-forming galaxies. Using low metallicity dwarf galaxies, De Looze et al. (2014) confirmed [CII] as a reliable SFR tracer. Moreover, the relation between [CII] and SFR does not appear to evolve significantly with redshift, making [CII] a robust SFR tracer even at high redshift (e.g. Schaerer et al. 2020; Pallottini et al. 2022).

[OIII] has a high ionization potential of 35.1 eV and arises mainly from ionized (HII) regions. Due to its relatively low critical density of 510 cm^{-3}, [OIII] does not dominate the cooling of ionized gas. However, as [OIII] originates from HII regions created by young stars, it still correlates with SFR (De Looze et al. 2014). In the local Universe, observations show that low-metallicity dwarfs are brighter in [OIII] than in [CII] (Cormier et al. 2012; Madden et al. 2013). As distant galaxies are expected to be less metal-enriched, the [OIII] line is predicted to be brighter than [CII] for $z > 8$ galaxies (Inoue et al. 2014b) and observed [OIII]/[CII] luminosity ratios are often in excess of one (e.g. Bakx et al. 2020; Schouws et al. 2025a).

1.2.3 Star formation rate density

Combining SFRs from large galaxy samples across different epochs in the history of the Universe can be especially insightful. This is closely tied to galaxy evolution, for example, by tracing the consumption of gas over time. Therefore, the star formation rate density (SFRD), the star formation rate per unit volume, is examined as a function of cosmic time.

The first measurements of the SFRD were carried out in the 1990s and revealed a decline in the SFRD from $z = 1$ to the present day (Lilly et al. 1996). Subsequent measurements of the SFRD showed a peak in star formation at $z \approx 2-3$ and a decline further back in time (Madau & Dickinson 2014). The overall shape of the cosmic star formation history is thought to be driven mostly by the interplay of gas accretion and feedback processes, which are dependent on the galaxy mass (Madau & Dickinson 2014). Measurements of the molecular gas mass density support this picture, as it peaks at a similar redshift as the SFRD (Walter et al. 2020).

The evolution of the SFRD obtained from observations in the rest-UV

and IR is shown in Figure 1.3. A clear discrepancy is seen between the measurements taken in the rest-UV and IR: at $z < 2$ the IR observations predict a SFRD that is higher by $\gtrsim 0.5$ dex. This highlights the importance of accounting for dust-obscured star formation in order to have a complete picture of the cosmic star formation history. Going further back in time, galaxies are younger and have had less time to build-up large dust reservoirs. It is therefore expected that the contribution of obscured star formation declines at higher redshift.

However, exactly how dusty the early Universe was is uncertain due to the scarcity of measurements at $z > 4$, especially in the IR. Historically, high-redshift measurements of the SFRD relied on rest-UV observations, biasing our view of the SFRD to unobscured, UV-bright galaxies. Recent work has found that the contribution of dust-obscured star formation in the early Universe is significant: at $z \sim 4.5-7$ the dust-obscured star formation could account for as much as $\sim 30-40\%$ of the total SFRD (Talia et al. 2021; Algera et al. 2023). To fully understand the contribution of obscured star formation as a function of cosmic time, large galaxy samples are needed that are preferentially unbiased to unobscured star formation.

1.3 Galaxy samples

1.3.1 REBELS

The Reionization Era Bright Emission Line Survey (REBELS) is an ALMA Large Program targeting 40 UV-bright galaxies ($-23 < \mathrm{M_{UV}} \leq -21.5$) at $z > 6.5$ (Bouwens et al. 2022b). The primary goal of REBELS was to identify and characterize a large sample of luminous galaxies in the EoR. To this end, depending on the redshift likelihood function of each source, either the [CII] or [OIII] line is targeted through spectral scans. For the majority of the galaxies, the [CII] emission line is targeted, while for the four highest-redshift sources ($z \geq 7.6$) [OIII] was expected to be more efficient to detect. In addition to the far-IR emission lines, the ALMA observations probe the dust continuum emission, providing constraints on the dust SEDs and the obscured star formation.

The REBELS ALMA observations yielded 25 [CII] detections (Bouwens et al. 2022b, Schouws et al., in prep), while none of the four [OIII] targets were detected (van Leeuwen et al. 2025, presented in Chapter 3). Dust continuum emission was successfully detected in 18 galaxies (Inami et al. 2022), making the REBELS survey a key galaxy sample to investigate dust-obscured star formation in UV-bright galaxies in the EoR. Later in cosmic time, at $4 < z < 6$, the ALPINE survey provided a large sample of 75 [CII]-detected, UV-bright sources (Le Fèvre et al. 2020; Béthermin et al. 2020). REBELS extends this work to higher redshifts and has led to nu-

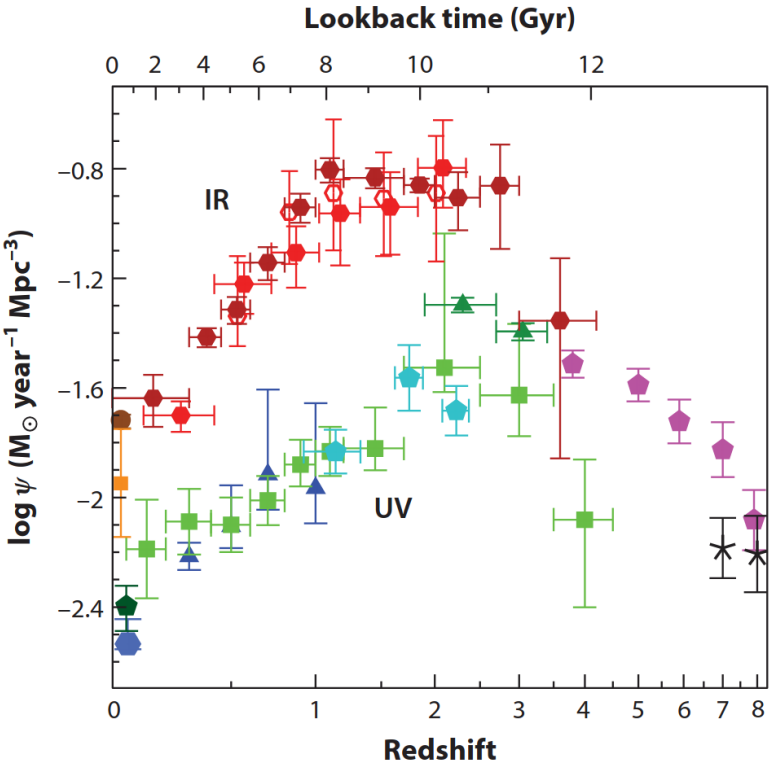

Figure 1.3: The evolution of the cosmic star formation rate density (SFRD) as a function of the redshift (or lookback time). Measurements in the IR are shown by the red, orange and brown data points, whereas rest-UV measurements are shown in blue, green and black. The magenta points are from rest-UV observations that have been explicitly corrected for dust attenuation. At $0 < z < 2$ the IR-based SFRD is $\gtrsim 0.5$ dex larger than that from rest-UV observations, indicating the significant contribution of dust-obscured star formation to the total SFRD. Due to the scarcity of measurements at $z > 4$, it is unclear exactly how important dust-obscured star formation is for understanding the star formation history of the early Universe. Figure from Madau & Dickinson (2014).

merous follow up ALMA programs and complementary *JWST* observations. As a result, REBELS has become an essential reference sample of massive galaxies in the EoR.

1.3.2 Companion galaxies

The discovery of serendipitously identified line emitters dates back more than a decade, when ALMA [CII] observations of BR1202−0725 at $z = 4.7$ showed that the IR bright source consists of a submillimeter galaxy, a quasar, as well as two companion galaxies (Carilli et al. 2013). Quasars were expected to be in especially overdense environments and this was spectroscopically confirmed with additional [CII] line detections in the field of view of many UV-bright quasars. An example of such a [CII]-emitter from Decarli et al. (2017) is shown in Figure 1.4 that has an observed frequency nearly identical to that of the quasar. Interestingly, while the quasar is clearly visible in the rest-UV, the serendipitously detected companion is completely undetected at these wavelengths. In the following years, the number of such quasar companions increased, establishing quasars as efficient environments for finding companion galaxies. For instance, Venemans et al. (2020) targeted 27 quasars and detected at least one [CII] companion for 13 of them.

However, companion galaxies are not limited to quasar environments. Both the REBELS and ALPINE surveys revealed [CII]-emitters in the neighborhood of UV-bright galaxies (Fudamoto et al. 2021; Loiacono et al. 2021; van Leeuwen et al. 2024). Three serendipitously [CII]-emitters were discovered in the ALMA observations of the REBELS survey. Two of these galaxies appeared to be consistent with normal, main-sequence star formation, and are heavily dust-obscured (Fudamoto et al. 2021).

Not all companion galaxies are as dust-obscured as these REBELS sources, but these findings indicate that there might be a significant amount of dust-obscured star formation missed by a rest-UV selection. The selection of galaxies through [CII] line emission seems a promising method to circumvent biasing samples to unobscured star formation. Since galaxies cluster, the detection of a [CII] line at a similar observed frequency as that of a UV-bright target suggests that the companion resides at the same redshift. This approach of selecting high redshift galaxies does not require dedicated observations, as existing observations of quasars or galaxies with secure redshifts can be utilized, making it a relatively cheap method. These results therefore motivate the use of serendipitously detected [CII]-emitters to constrain the contribution of dust-obscured star formation at high redshift.

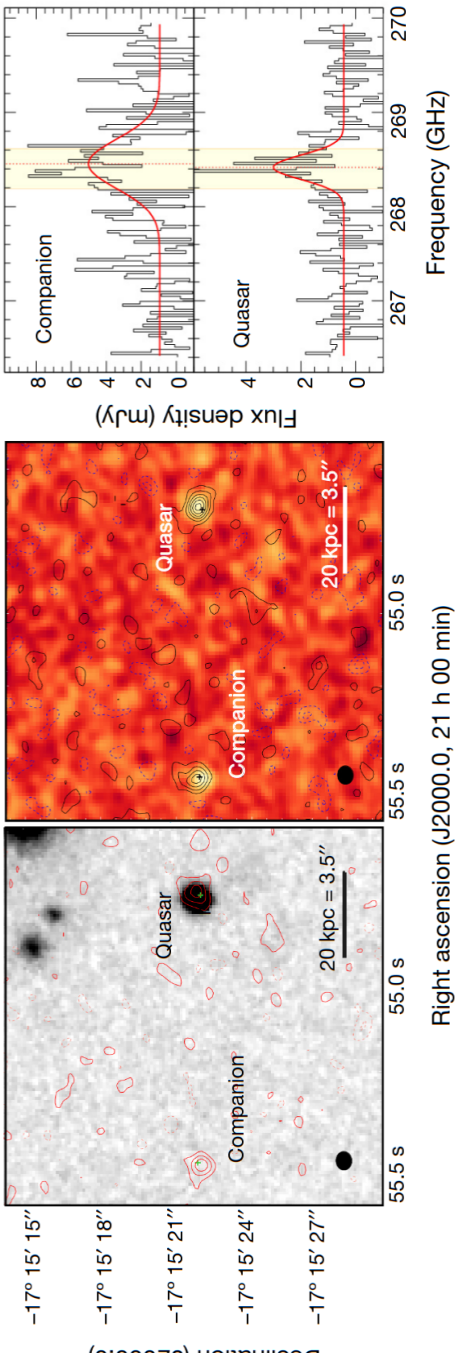

Figure 1.4: *Left:* rest-UV observations of a quasar (J2100-1715, $z = 6.08$) and a serendipitously detected [CII]-emitter (J-band of the Large Binocular Telescope (LBT)). While the quasar is bright in the rest-UV and clearly detected, the companion is completely invisible. The overlaying red contours show the dust continuum emission at 1.2 mm. *Center:* the ALMA 1.2 mm continuum map with black contours indicating the [CII] line emission. *Right:* The spectra of the companion and the quasar indicating that the [CII] lines are at nearly identical frequencies (Δv $= -40$ km s^{-1}), and therefore that they are likely at the same redshift. Figure adapted from Decarli et al. (2017).

1.4 Instruments

1.4.1 Atacama Large Millimeter/Submillimeter Array

The Atacama Large Millimeter/Submillimeter Array (ALMA) (Wootten & Thompson 2009) is an interferometer antenna array located on the Chajnantor plateau in Chile at an elevation of 5000 meter. The site's high altitude and dry environment facilitates observations in the millimeter and submillimeter regime, where atmospheric water vapor otherwise limits transmission. ALMA consists of a main array of fifty 12-meter antennas, the Atacama Compact Array comprised of twelve 7-meter antennas and four 12-meter antennas utilized in the Total Power Array.

Since beginning scientific operations in 2011, ALMA has made an enormous impact on the study of high redshift galaxies (Hodge & da Cunha 2020). Compared to previous instruments operating at similar wavelengths (e.g. SCUBA), ALMA reaches much higher sensitivity and angular resolution, reducing source confusion and enabling detections of sources fainter than merely bright submillimeter galaxies. At $z > 4$ ALMA covers the rest-frame frequencies of a wide range of emission lines, including high-J CO transitions, $[\mathrm{CII}]_{158\mu\mathrm{m}}$, $[\mathrm{OIII}]_{52\mu\mathrm{m}}$, $[\mathrm{OIII}]_{88\mu\mathrm{m}}$, $[\mathrm{NII}]_{122\mu\mathrm{m}}$ and $[\mathrm{NII}]_{205\mu\mathrm{m}}$ (see e.g. Carilli & Walter 2013). By targeting such lines, ALMA has been instrumental for spectroscopic redshift confirmations. Additionally, these line detections enable studies of galaxy dynamics as well as characterization of the ISM of high redshift galaxies.

Furthermore, due to ALMA's ability to detect dust continuum emission, it has been crucial for studying the obscured star formation in the early Universe. Notably, ALMA successfully detected the dust continuum in a galaxy at $z = 8.31$ (MACS0416_Y1; Tamura et al. 2019; Bakx et al. 2020; Tamura et al. 2023). For galaxies at $z > 4$, most ALMA observations are on the Rayleigh-Jeans tail of the dust SED. Obtaining constraints near the dust SED peak is challenging due to limited atmospheric transmission at higher frequencies and high integration times required. As a result, constraining the shape of the dust SED remains challenging, even with observations in multiple frequency bands.

The ongoing Wideband Sensitivity Upgrade (WSU) will significantly decrease the integration times needed for continuum detections by broadening the frequency range that can be observed simultaneously. This will facilitate more detections of the dust continuum of high redshift galaxies in the future. Additionally, the WSU will greatly decrease the time needed for spectral line scans, enabling the identification of more high redshift galaxies within a given integration time.

1.4.2 Hubble Space Telescope

The Hubble Space Telescope (*HST*) was launched in 1990 into a low-Earth orbit. The *HST* completes an orbit around the Earth every 95 minutes and is equipped with a 2.4-meter primary mirror. With the current operational instruments, *HST* covers wavelengths from $\sim 0.12 - 1.7\mu$m. Of particular relevance is the Wide Field Camera 3, which facilitates rest-UV observations of $4 < z < 6$ galaxies and therefore measurements of the unobscured star formation. Although ground-based facilities cover similar wavelengths, their sensitivity is limited by the atmosphere. For decades, *HST* therefore remained the only space telescope with the required sensitivity and resolution for the identification of large samples of UV-bright high-redshift galaxies. These observations have been instrumental for establishing how abundant UV-bright objects are (e.g. through UV luminosity functions; Bouwens et al. 2015), providing key insights into galaxy formation in the early Universe.

1.4.3 James Webb Space Telescope

On Christmas Day 2021 the James Webb Space Telescope (*JWST*) launched and roughly one month later arrived at the second Lagrange point. *JWST* observes in a broad wavelength range, from 0.6 μm to 28.3 μm, covering the rest-UV to near-IR light of high redshift galaxies. With a 6.5-meter primary mirror, its resolution and sensitivity are between three and a hundred times greater than previous facilities operating at similar wavelengths, such as *HST* (Rigby et al. 2023). The Near Infrared Camera (NIRCam), one of the four scientific instruments, is widely used to observe high redshift galaxies in $0.6 - 5.0$ μm. In addition to direct imaging, NIRCam is equipped with grisms that enable wide field slitless spectroscopy.

At the time of writing, *JWST* is at the forefront of the redshift frontier as its sensitivity allows identification of galaxies with much fainter rest-UV luminosities. The most distant spectroscopically confirmed galaxy is detected by *JWST* at $z = 14.44$ (MoM-z14; Naidu et al. 2025). Moreover, *JWST*'s coverage of IR wavelengths enables observations of the stellar continuum at longer wavelengths of high redshift galaxies, crucial for robustly determining stellar masses. *JWST* has been dramatically transforming our understanding of the early Universe. Already, it is challenging existing galaxy formation models by discovering a higher abundance of UV-bright galaxies than predicted (Adamo et al. 2025).

1.5 This thesis

With ALMA and *JWST*, we have entered a new era of observations of the early Universe. ALMA enables sensitive measurements of the dust-obscured

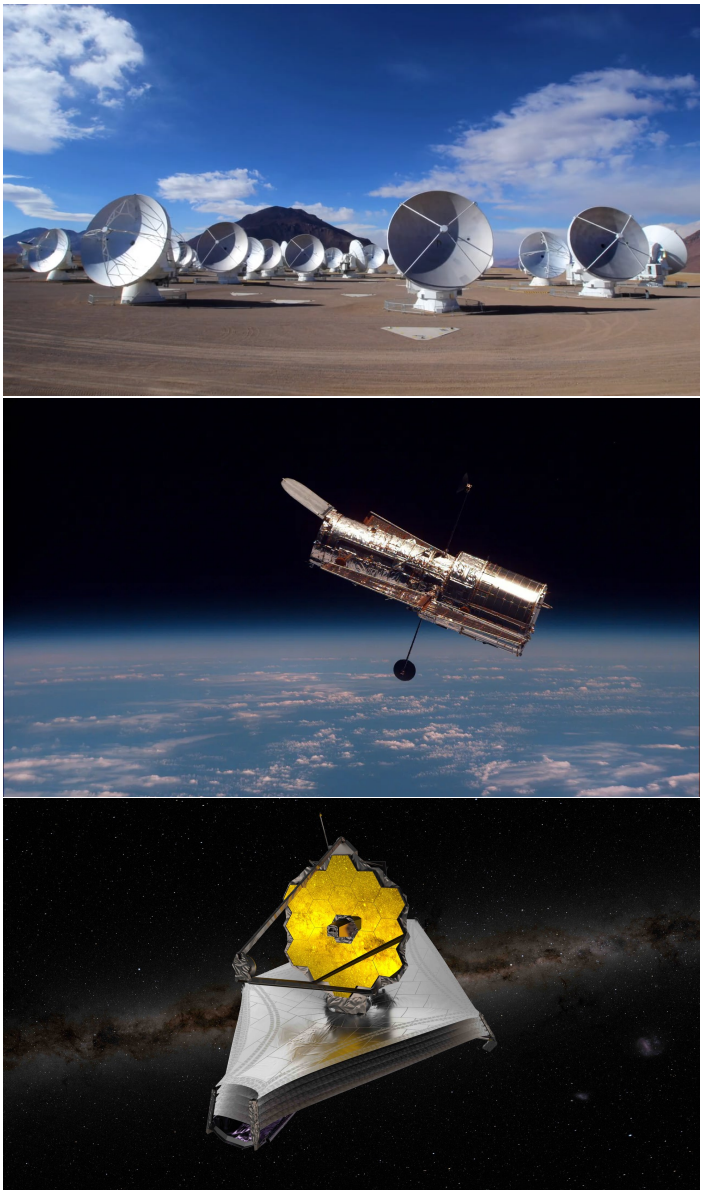

Figure 1.5: *Top:* The Atacama Large Millimeter/Submillimeter Array in the Atacama desert in Chile (ALMA (ESO/NAOJ/NRAO)). *Middle:* The Hubble Space Telescope captured in its orbit around Earth (NASA). *Bottom:* A visualization of the James Webb Space Telescope at the second Lagrange point (ESA/ATG medialab).

star formation, revealing dusty galaxies that would be invisible in the rest-UV. *JWST* is uncovering galaxies at previously unexplored redshifts and providing tight constraints on the unobscured star formation rate as well as stellar masses. In this thesis we leverage the complementary capabilities of these instruments to examine the properties of $z \geq 4$ galaxies and their dust-obscured star formation.

In **Chapter 2**, we present a novel method to infer the SFRD at $z \gtrsim 5$ using a sample of 18 serendipitously identified [CII] emitters. By utilizing companions discovered in ALMA [CII] observations of massive, UV-bright galaxies and quasars, we construct a SFR-selected sample that is unbiased to unobscured star formation. The high redshift companion galaxies are selected based on small velocity separations ($\leq$ 500 km s^{-1}) with respect to the UV-bright source, maximizing the likelihood that they reside at the same redshift. The [CII]-selected sample is utilized to characterize how much star formation is obscured as a function of the total SFR. The quasar companions seem to be significantly more obscured ($f_{\rm obs} \approx 93\%$) than galaxies around star-forming galaxies ($f_{\rm obs} \approx 63\%$). Furthermore, the companion sample is used to forward model the dust-corrected UV luminosity function. These results suggest that obscured star formation has a non-negligible contribution of $> 3-10\%$ of the total SFRD at $z \sim 5-6$.

In **Chapter 3**, we introduce the results of the [OIII] line scans of four $z \geq 7.6$ galaxies from the REBELS survey. No credible [OIII] detections were found for any of the four sources, although two sources are significantly ($\geq 3.8\sigma$) detected in the dust continuum. The non-detection of [OIII] is particularly notable for REBELS-04, where the ALMA observations cover $\geq$ 92% of the redshift likelihood function and the estimated SFR is 40 M$_\odot$ yr^{-1}. We examine the ISM conditions that could explain the non-detection of [OIII] and conclude that high ISM densities and/or low ionization parameters are likely responsible. If the photometric redshift of REBELS-04 is confirmed ($z_{\rm phot} = 8.57$), it would constitute the most distant dust-detected galaxy with ALMA. For another source, REBELS-37, dust continuum observations in two ALMA bands allow us to investigate the shape of the dust SED, excluding cold dust temperatures ($\lesssim$ 28 K).

In **Chapter 4**, we revisit the [CII]-selected companion sample of Chapter 2 with new *JWST* NIRCam observations. For nine companion galaxies we constrain the rest-UV/optical photometry with HSC, *HST* and *JWST* observations. To infer whether we correctly interpret the ALMA line emission as [CII], we derive redshift likelihood distributions and find that six out of nine companions are almost certainly at $z > 4$ indicating that [CII] is observed. Using SED modeling, we derive the stellar masses of the companions and find that the majority are on the star-forming main sequence. We find a wide range of fractions of obscured star formation for the [CII]-selected galaxies, from $<$ 67% to 100%. Making use of NIRCam grism observations, we examine the selectability of obscured galaxies using the [OIII]$_{4959,5007}$

doublet and find that the doublet may not be seen at sufficiently high S/N for obscured galaxies to be easily identified in JWST grism surveys. We find that a [CII] selection yields an representative selection of galaxies on the upper end of the star-forming main sequence at $z > 4$. The serendipitously identified galaxies thus provide us with a valuable tool for characterizing obscured star formation in the early Universe.